Cite as: B. B. He *et al.*, *Science* 10.1126/science.aan0177 (2017).

# High dislocation density–induced large ductility in deformed and partitioned steels

**B. B. He,[1] B. Hu,[2] H. W. Yen,[3] G. J. Cheng,[3] Z. K. Wang,[4] H. W. Luo,[2]* M. X. Huang[1]***

[1]Department of Mechanical Engineering, The University of Hong Kong, Hong Kong, China. [2]School of Metallurgical and Ecological Engineering, University of Science and Technology Beijing, Xue Yuan Lu 30, Beijing 100083, China. [3]Department of Materials Science and Engineering, National Taiwan University, Taiwan. [4]Department of Mechanical and Biomedical Engineering, City University of Hong Kong, Hong Kong 999077, China.

*Corresponding author. Email: mxhuang@hku.hk (M.X.H.); luohaiwen@ustb.edu.cn (H.W.L.)

**A wide variety of industrial applications require materials with high strength and ductility. Unfortunately, the strategies for increasing material strength, such as processing to create line defects (dislocations), tend to decrease ductility. We developed a strategy to circumvent this in inexpensive, medium Mn steel. Cold rolling followed by low-temperature tempering developed steel with metastable austenite grains embedded in a highly dislocated martensite matrix. This deformed and partitioned (D&P) process produced dislocation hardening, but retained high ductility both through the glide of intensive mobile dislocations and by allowing us to control martensitic transformation. The D&P strategy should apply to any other alloy with deformation-induced martensitic transformation and provides a pathway for development of high strength, high ductility materials.**

Strength and ductility are key mechanical properties of metallic materials for developing energy-efficient and lightweight structural components in a wide variety of industries, including automotive and aerospace. Unfortunately, improving strength or ductility often results in the degradation of the other property, which is known as the strength-ductility trade-off (*1*). Cost is also an issue as alloying elements that help improve both properties, such as cobalt and titanium, tend to be expensive. Previous efforts towards resolving this trade-off focused on engineering defects like grain boundaries (*2*, *3*) and coherent twin-boundaries (*4*, *5*). However, the strength may reach a limit when grain size or twin-boundary spacing is reduced to nanometers (*6*–*8*). Dislocations or line defects are a different pathway for engineering alloy properties. In contrast to the above planar defects, the strength of metallic materials monotonically increases with dislocation density according to the well-known Taylor hardening law (*9*). The problem is that ductility tends to decrease as the number of dislocations increase. However, improved choices in alloy composition and clever processing strategies may allow dislocation engineering to circumvent the strength-ductility trade-off. In particular, achieving large ductility in the presence of high dislocation density in an inexpensive material produced by facile processing routes is desirable for broad industrial applications at an economic cost.

Severe plastic deformation (SPD) or phase transformation both generate high dislocation density in metals. Cold drawing is one SPD that introduces a very high dislocation density in pearlitic steel wires (*10*). Cold drawing and other SPD methods also may lead to grain refinement (<100 nm) in metals due to formation of high angle grain boundaries by re-arrangement of intensive dislocations (*10*, *11*). In contrast, the first order solid state martensitic transformation produces a highly dislocated martensite microstructure without a lot of grain refinement (~500 nm) in steels (*12*). Either quenching or deformation can trigger martensitic transformation, depending on the alloying content of steels (*13*, *14*). We show that rolling and low temperature tempering produced a high dislocation density in steel, also enabling a large ductility. In addition to the high dislocation density, interstitial C atoms partition into and help stabilize the austenite phase during tempering (*13*). We define this thermomechanical treatment as "deformed and partitioned (D&P)" process and the corresponding steel as D&P steel. The D&P process could be realized with conventional processing techniques that are compatible with existing industrial production lines.

We used a medium Mn steel (10% Mn, 0.47% C, 2% Al and 0.7% V (wt.%)) for the D&P process. The Mn and C atoms are effective austenite stabilizers (fig. S1). The addition of 2% Al content is to suppress cementite precipitation during tempering process. The addition of 0.7% V is to form intensive nanometer-sized V carbides which provided enhanced resistance to delayed fracture induced by hydrogen embrittlement (*15*, *16*). The D&P steel that we produced by multiple deformation and annealing steps (*17*) possesses a heterogeneous lamella dual-phase microstructure in which metastable austenite are embedded in a martensite matrix (Fig. 1A). We obtained the martensite matrix by cold rolling (fig. S2) followed by tempering. The tempered martensite matrix has heterogeneous grain morphologies and sub-

structures. Large lenticular martensite grains, which constitute the majority of matrix, are mainly decorated with dislocation cells (Fig. 1B). Nevertheless, some large lenticular martensite grains also possess dislocations as well as twins (Fig. 1C) and some small lath martensite grains with dislocations (Fig. 1D) in the martensite matrix. We estimated the average dislocation density of martensite matrix (~$1.27\times10^{16}$ $m^{-2}$) with synchrotron X-ray diffraction (XRD) (fig. S3). Such a high dislocation density is due to the combination of plastic deformation and displacive shear transformation. The martensite we created differs from the thermally formed martensite obtained by quenching as it inherits dislocations generated from warm deformation. The early transformed martensite is also subjected to cold rolling, which we confirmed by the formation of dislocation cells in martensite (Fig. 1B) (*18*). Consequently, the dislocation density in our martensite matrix is much larger than for thermally formed martensite (~$2.36\times10^{14}$ $m^{-2}$) (fig. S3). The austenite phase also has a heterogeneous microstructure, including coarse lamella grains (Fig. 1A), ultrafine lamella grains (Fig. 1D) and sub-micron granular grains (Fig. 1E). The large austenite grains are decorated with a large number of dislocations as well as stacking faults (Fig. 1F), while the small austenite grains mainly possess dislocations (Fig. 1E). Both martensite and austenite phases contain nanometer-sized vanadium carbides (Fig. 1, G and H) and solid solutes (C, Mn and V atoms). Although some layered austenite grains have higher Mn content (fig. S4) from the banding of Mn in hot rolled strip (fig. S1), we also observed austenite grains with low Mn content and martensite with high Mn content (fig. S4). This suggests that the Mn banding does not determine retention of the layered austenite grains in the D&P steel. Instead, it could be due to the mechanical stabilization induced by intensive defects in these layered austenite grains (Fig. 1F) (*19*).

The as-developed D&P steel possessed an ultra-high yield strength of 2.21 GPa and 2.05 GPa (Fig. 2). The high yield strength is from the high dislocation density ($\rho_t$) in the martensite matrix. For instance, the yield stress ($\sigma$) due to dislocation forest strengthening is estimated to be 1.6 GPa according to Taylor hardening law (*9*)

$$\sigma = M\alpha\mu b\sqrt{\rho_t} \quad (1)$$

where Taylor factor $M$ is 2.9 (*20*), the empirical constant $\alpha$ is 0.23 for cell-forming dislocation distribution (*21*), shear modulus $\mu$ is 85 GPa (*22*) and Burgers vector $b$ is 0.25 nm (*20*). Therefore, the yield stress induced by the high dislocation density is on the same order of magnitude as the macroscopic yield strength (Fig. 2). The collective contributions from the other strengthening defects, such as solid solutes, nano-precipitates, stacking faults, twin boundaries and ultrafine grains (Fig.1), elevated the yield strength beyond 2 GPa. Consequently, the D&P steel has a higher yield strength than steel with a bimodal coarse-grained microstructure (Fig. 2 and fig. S5). Intriguingly, the D&P steel also had a larger tensile uniform elongation (>15%) than its bimodal coarse-grained counterpart. Our D&P steel with high dislocation density has an inverse strength-ductility tradeoff similar to what has been found in other materials (*23*).

The high dislocation density in our D&P steel results in an ultra-high yield strength. The large uniform elongation is also due to the dislocation density. The D&P steel demonstrates discontinuous yielding followed by large Lüders strains ($\varepsilon$) (Fig. 2). The enhanced yield drop after the prolonged annealing is a typical feature of strain aging during which both mobile and immobile dislocations are segregated by solid solutes (*24*). Martensite has an inherently high ratio (~18%) of mobile screw dislocations from displacive shear transformations (*25*, *26*). The mobile and immobile dislocations in martensite could re-arrange to form dislocation cells (Fig. 1B) during cold rolling, while the characteristics of dislocations remain the same (*18*, *27*). The dislocation cells consist of cell interior with low dislocation density and cell wall with high dislocation density. The catastrophic release and glide of the mobile screw dislocations from the cell wall leads to the collapse and break of original cell boundaries and formation of elongated dislocation cell structure after Lüders strain, which we confirmed by comparing Fig. 1B and Fig. 3A. The elongated cell has an increased length of ~400 nm compared to the original cell structure, which indicates that the average glide distance of the mobile screw dislocations is ~400 nm. A general relationship between plastic strain and mobile dislocation density ($\rho_m$) can be written as (*28*)

$$\varepsilon = \rho_m b L/M \quad (2)$$

where $L$ is the average glide distance of the mobile dislocations (~400 nm). We assumed the ratio of mobile dislocation density to total dislocation density is 18% for deformation-induced martensite (*26*), given a mobile dislocation density of $2.3\times10^{15}$ $m^{-2}$ in the martensite matrix. Consequently, the plastic strain induced by glide of these mobile dislocations in the martensite matrix is estimated to be 6.8%, which constitutes to a large portion of measured Lüders strain (7%~9%) in the D&P steel (Fig. 2). The high mobile dislocation density in the martensite matrix accommodates a large plasticity upon yielding. The catastrophic release and glide of the mobile screw dislocations result in a low but positive strain hardening rate during Lüders strain regime (fig. S6). Such a low but positive strain hardening rate has been reported in irradiated metals (*29*) and omega-containing Ti-alloys (*30*), in which the operation of dislocation channeling is the governing deformation mechanism.

Besides the high mobile dislocation density, the D&P steel had a continuous transformation-induced plasticity (TRIP) effect at a large strain during the tensile test (Fig.

3B). The TRIP effect resulted from the formation of martensite in the coarse layered austenite grains. This TRIP effect applied compressive residual stress to effectively blunt localized plasticity during tensile straining (fig. S7) (*31*), and also provided dynamic strain partitioning between phases and improved strain hardening (fig. S6) (*32*). The formation of the large martensite grains suggests that coarse layered austenite grains are less stable than ultra-fine austenite grains during uni-axial tensile deformation (Fig. 3C). Nevertheless, most of these coarse layered austenite grains only transform to martensite at strains beyond the Lüders strain (Fig. 3B), suggesting their high mechanical stability in the D&P steel. We ascribed the enhancement in the mechanical stability to the high dislocation density in large austenite grains (Fig. 1F) where dislocations can act as barriers for glissile martensite interface and therefore stabilize austenite grains (*19*). Moreover, the hard martensite matrix (fig. S8) can shield austenite from deformation (*33*), allowing the austenite to transform at large strain regime. The austenite grains in the D&P steel were further stabilized by C partitioning from martensite (fig. S9) (*13*) relative to the ones in deformed steel (fig. S10). Besides the effect of C partitioning and relatively higher Mn content (fig. S4), the high dislocation density in the D&P steel also controlled release of TRIP effect, improving ductility.

The D&P steel also had a twinning-induced plasticity (TWIP) effect during the tensile test. We mostly observed the TWIP effect, induced by the formation of deformation twins, in ultra-fine austenite grains (Fig. 3D). The initiation of nanotwins from phase boundary suggests a high stress level experienced by lamella austenite grain (Fig. 3D). Therefore, the TWIP effect also operated in the large strain regime (fig. S6). The minor austenite volume fraction (Fig. 1A) of the small grains means we expect the TWIP effect to be much less important than the TRIP effect, even as deformation twins can accumulate deformations and improve ductility (*4*).

We compared the bulk properties of D&P steel to other high strength metallic materials (Fig. 4). The D&P steel exhibits a yield strength that is 50% higher than that of nanobainite steel while maintaining a comparable uniform elongation (Fig. 4). Moreover, it exhibits a uniform elongation that is one order of magnitude larger than that of commercial maraging steels while maintaining an equivalent yield strength. Consequently, our D&P steel achieves excellent tensile properties and defines a new space in the strength-ductility map (Fig. 4). Despite of its discontinuous yielding and Lüders strain (Fig. 2), the ultra-high yield strength of our D&P steel makes it a desirable alloy for applications where yield strength is the main design criteria.

The D&P overcomes the challenge of creating martensite known to be an issue for compositionally similar steels that rely on a quenching and partitioning process (*13*) (fig. S5). The high dislocation density in the D&P steel not only increases the yield strength by dislocation forest hardening but also enables a large ductility by the glide of existing mobile dislocations and by the controlled release of TRIP effect. The high dislocation density is the origin of the inverse strength-ductility trade-off. We expect this strategy will be useful in other systems with similar deformation-induced martensitic transformation mechanism such as titanium alloys (*34*). The D&P steel exhibits low raw materials cost as compared to the maraging steel while maintaining a comparable ultimate tensile strength (fig. S11). Therefore, by engineering dislocations, we simultaneously alleviate the economic concerns while achieving ultra-high strength.

## REFERENCES AND NOTES


1. Y. Wei, Y. Li, L. Zhu, Y. Liu, X. Lei, G. Wang, Y. Wu, Z. Mi, J. Liu, H. Wang, H. Gao, Evading the strength-ductility trade-off dilemma in steel through gradient hierarchical nanotwins. *Nat. Commun.* **5**, 3580 (2014). doi:10.1038/ncomms4580 Medline
2. Y. Wang, M. Chen, F. Zhou, E. Ma, High tensile ductility in a nanostructured metal. *Nature* **419**, 912–915 (2002). doi:10.1038/nature01133 Medline
3. X. Wu, M. Yang, F. Yuan, G. Wu, Y. Wei, X. Huang, Y. Zhu, Heterogeneous lamella structure unites ultrafine-grain strength with coarse-grain ductility. *Proc. Natl. Acad. Sci. U.S.A.* **112**, 14501–14505 (2015). doi:10.1073/pnas.1517193112 Medline
4. L. Lu, Y. Shen, X. Chen, L. Qian, K. Lu, Ultrahigh strength and high electrical conductivity in copper. *Science* **304**, 422–426 (2004). doi:10.1126/science.1092905 Medline
5. K. Lu, L. Lu, S. Suresh, Strengthening materials by engineering coherent internal boundaries at the nanoscale. *Science* **324**, 349–352 (2009). doi:10.1126/science.1159610 Medline
6. J. Schiøtz, F. D. Di Tolla, K. W. Jacobsen, Softening of nanocrystalline metals at very small grain sizes. *Nature* **391**, 561–563 (1998). doi:10.1038/35328
7. X. Li, Y. Wei, L. Lu, K. Lu, H. Gao, Dislocation nucleation governed softening and maximum strength in nano-twinned metals. *Nature* **464**, 877–880 (2010). doi:10.1038/nature08929 Medline
8. L. Lu, X. Chen, X. Huang, K. Lu, Revealing the maximum strength in nanotwinned copper. *Science* **323**, 607–610 (2009). doi:10.1126/science.1167641 Medline
9. G. I. Taylor, The mechanism of plastic deformation of crystals. Part I. Theoretical. *Proc. R. Soc. London A Contain. Pap. Math. Phys. Character* **145**, 362–387 (1934). doi:10.1098/rspa.1934.0106
10. X. Zhang, A. Godfrey, X. Huang, N. Hansen, Q. Liu, Microstructure and strengthening mechanisms in cold-drawn pearlitic steel wire. *Acta Mater.* **59**, 3422–3430 (2011). doi:10.1016/j.actamat.2011.02.017
11. R. Z. Valiev, R. K. Islamgaliev, I. V. Alexandrov, Bulk nanostructured materials from severe plastic deformation. *Prog. Mater. Sci.* **45**, 103–189 (2000). doi:10.1016/S0079-6425(99)00007-9
12. S. Morito, X. Huang, T. Furuhara, T. Maki, N. Hansen, The morphology and crystallography of lath martensite in alloy steels. *Acta Mater.* **54**, 5323–5331 (2006). doi:10.1016/j.actamat.2006.07.009
13. J. Speer, D. Matlock, B. De Cooman, J. Schroth, Carbon partitioning into austenite after martensite transformation. *Acta Mater.* **51**, 2611–2622 (2003). doi:10.1016/S1359-6454(03)00059-4
14. G. Olson, M. Cohen, Kinetics of strain-induced martensitic nucleation. *Metall. Trans. A Phys. Metall. Mater. Sci.* **6**, 791–795 (1975). doi:10.1007/BF02672301
15. K. Kawakami, T. Matsumiya, Numerical analysis of hydrogen trap state by TiC and $V_4C_3$ in bcc-Fe. *ISIJ Int.* **52**, 1693–1697 (2012). doi:10.2355/isijinternational.52.1693
16. Y.-S. Chen, D. Haley, S. S. A. Gerstl, A. J. London, F. Sweeney, R. A. Wepf, W. M. Rainforth, P. A. J. Bagot, M. P. Moody, Direct observation of individual hydrogen atoms at trapping sites in a ferritic steel. *Science* **355**, 1196–1199 (2017).

doi:10.1126/science.aal2418 Medline
17. Materials and methods are available as supplementary materials.
18. D. Akama, T. Tsuchiyama, S. Takaki, Change in dislocation characteristics with cold working in ultralow-carbon martensitic steel. *ISIJ Int.* **56**, 1675–1680 (2016). doi:10.2355/isijinternational.ISIJINT-2016-140
19. S. Chatterjee, H. S. Wang, J. R. Yang, H. K. D. H. Bhadeshia, Mechanical stabilisation of austenite. *Mater. Sci. Technol.* **22**, 641–644 (2006). doi:10.1179/174328406X86128
20. M. Sauzay, B. Fournier, M. Mottot, A. Pineau, I. Monnet, Cyclic softening of martensitic steels at high temperature—Experiments and physically based modelling. *Mater. Sci. Eng. A* **483-484**, 410–414 (2008). doi:10.1016/j.msea.2006.12.183
21. T. Ungár, A. D. Stoica, G. Tichy, X.-L. Wang, Orientation-dependent evolution of the dislocation density in grain populations with different crystallographic orientations relative to the tensile axis in a polycrystalline aggregate of stainless steel. *Acta Mater.* **66**, 251–261 (2014). doi:10.1016/j.actamat.2013.11.012
22. F. Lani, Q. Furnémont, T. Van Rompaey, F. Delannay, P. J. Jacques, T. Pardoen, Multiscale mechanics of TRIP-assisted multiphase steels: II. Micromechanical modelling. *Acta Mater.* **55**, 3695–3705 (2007). doi:10.1016/j.actamat.2007.02.015
23. Z. Li, K. G. Pradeep, Y. Deng, D. Raabe, C. C. Tasan, Metastable high-entropy dual-phase alloys overcome the strength-ductility trade-off. *Nature* **534**, 227–230 (2016). Medline
24. A. H. Cottrell, B. Bilby, Dislocation theory of yielding and strain ageing of iron. *Proc. R. Soc. London Ser. A* **62**, 49–62 (1949). doi:10.1088/0370-1298/62/1/308
25. B. Sandvik, C. Wayman, Characteristics of lath martensite: Part I. Crystallographic and substructural features. *MTA* **14**, 809–822 (1983). doi:10.1007/BF02644284
26. T. Hatem, M. Zikry, A model for determining initial dislocation-densities associated with martensitic transformations. *Mater. Sci. Technol.* **27**, 1570–1573 (2013).
27. T. Shintani, Y. Murata, Evaluation of the dislocation density and dislocation character in cold rolled Type 304 steel determined by profile analysis of X-ray diffraction. *Acta Mater.* **59**, 4314–4322 (2011). doi:10.1016/j.actamat.2011.03.055
28. J. Hirth, J. Lothe, *Theory of Dislocations* (Wiley, 1982).
29. M. Victoria, N. Baluc, C. Bailat, Y. Dai, M. I. Luppo, R. Schäublin, B. N. Singh, The microstructure and associated tensile properties of irradiated fcc and bcc metals. *J. Nucl. Mater.* **276**, 114–122 (2000). doi:10.1016/S0022-3115(99)00203-2
30. M. Lai, C. C. Tasan, D. Raabe, Deformation mechanism of ω-enriched Ti–Nb-based gum metal: Dislocation channeling and deformation induced ω–β transformation. *Acta Mater.* **100**, 290–300 (2015). doi:10.1016/j.actamat.2015.08.047
31. M. Koyama, Z. Zhang, M. Wang, D. Ponge, D. Raabe, K. Tsuzaki, H. Noguchi, C. C. Tasan, Bone-like crack resistance in hierarchical metastable nanolaminate steels. *Science* **355**, 1055–1057 (2017). doi:10.1126/science.aal2766 Medline
32. M.-M. Wang, C. C. Tasan, D. Ponge, A.-C. Dippel, D. Raabe, Nanolaminate transformation-induced plasticity–twinning-induced plasticity steel with dynamic strain partitioning and enhanced damage resistance. *Acta Mater.* **85**, 216–228 (2015). doi:10.1016/j.actamat.2014.11.010
33. P. J. Jacques, F. Delannay, J. Ladrière, On the influence of interactions between phases on the mechanical stability of retained austenite in transformation-induced plasticity multiphase steels. *Metall. Mater. Trans. A Phys. Metall. Mater. Sci.* **32**, 2759–2768 (2001). doi:10.1007/s11661-001-1027-4
34. S. Neelakantan, E. I. Galindo-Nava, D. San Martin, J. Chao, P. E. J. Rivera-Díaz-del-Castillo, Modelling and design of stress-induced martensite formation in metastable β Ti alloys. *Mater. Sci. Eng. A* **590**, 140–146 (2014). doi:10.1016/j.msea.2013.10.003
35. X. Wang, L. Wang, M. Huang, Kinematic and thermal characteristics of Lüders and Portevin-Le Châtelier bands in a medium Mn transformation-induced plasticity steel. *Acta Mater.* **124**, 17–29 (2017). doi:10.1016/j.actamat.2016.10.069
36. C. García-Mateo, F. G. Caballero, The role of retained austenite on tensile properties of steels with bainitic microstructures. *Mater. Trans.* **46**, 1839–1846 (2005). doi:10.2320/matertrans.46.1839
37. Nickel Development Institute, "18 per cent nickel maraging steels: Engineering properties" (Publication 4419, Inco Europe Limited, London, 1976).
38. S. Jiang, H. Wang, Y. Wu, X. Liu, H. Chen, M. Yao, B. Gault, D. Ponge, D. Raabe, A. Hirata, M. Chen, Y. Wang, Z. Lu, Ultrastrong steel via minimal lattice misfit and high-density nanoprecipitation. *Nature* **544**, 460–464 (2017). doi:10.1038/nature22032 Medline
39. O. Bouaziz, H. Zurob, M. Huang, Driving force and logic of development of advanced high strength steels for automotive applications. *Steel Res. Int.* **84**, 937–947 (2013).
40. A. Arlazarov, O. Bouaziz, A. Hazotte, M. Gouné, S. Allain, Characterization and modeling of manganese effect on strength and strain hardening of martensitic carbon steels. *ISIJ Int.* **53**, 1076–1080 (2013). doi:10.2355/isijinternational.53.1076
41. J. Zhao, Y. Xi, W. Shi, L. Li, Microstructure and mechanical properties of high manganese TRIP steel. *J. Iron Steel Res. Int.* **19**, 57–62 (2012). doi:10.1016/S1006-706X(12)60088-0
42. M. Zhang, L. Li, R. Fu, D. Krizan, B. De Cooman, Continuous cooling transformation diagrams and properties of micro-alloyed TRIP steels. *Mater. Sci. Eng. A* **438-440**, 296–299 (2006). doi:10.1016/j.msea.2006.01.128
43. E. D. Moor, J. G. Speer, D. K. Matlock, J.-H. Kwak, S.-B. Lee, Effect of carbon and manganese on the quenching and partitioning response of CMnSi steels. *ISIJ Int.* **51**, 137–144 (2011). doi:10.2355/isijinternational.51.137
44. H. Wang, N. Tao, K. Lu, Strengthening an austenitic Fe–Mn steel using nanotwinned austenitic grains. *Acta Mater.* **60**, 4027–4040 (2012). doi:10.1016/j.actamat.2012.03.035
45. O. Bouaziz, D. Barbier, P. Cugy, G. Petigand, Effect of process parameters on a metallurgical route providing nano-structured single phase steel with high work-hardening. *Adv. Eng. Mater.* **14**, 49–51 (2012). doi:10.1002/adem.201100164
46. D. Raabe, D. Ponge, O. Dmitrieva, B. Sander, Nanoprecipitate-hardened 1.5 GPa steels with unexpected high ductility. *Scr. Mater.* **60**, 1141–1144 (2009). doi:10.1016/j.scriptamat.2009.02.062
47. S.-H. Kim, H. Kim, N. J. Kim, Brittle intermetallic compound makes ultrastrong low-density steel with large ductility. *Nature* **518**, 77–79 (2015). doi:10.1038/nature14144 Medline
48. J. He, H. Wang, H. L. Huang, X. D. Xu, M. W. Chen, Y. Wu, X. J. Liu, T. G. Nieh, K. An, Z. P. Lu, A precipitation-hardened high-entropy alloy with outstanding tensile properties. *Acta Mater.* **102**, 187–196 (2016). doi:10.1016/j.actamat.2015.08.076
49. C.-W. Tsai, M.-H. Tsai, K.-Y. Tsai, S.-Y. Chang, J.-W. Yeh, A.-C. Yeh, Microstructure and tensile properties of $Al_{0.5}CoCrCuFeNi$ alloys produced by simple rolling and annealing. *Mater. Sci. Technol.* **31**, 1178–1183 (2015). doi:10.1179/1743284714Y.0000000754
50. Q. Wei, L. Kecskes, Effect of low-temperature rolling on the tensile behavior of commercially pure tungsten. *Mater. Sci. Eng. A* **491**, 62–69 (2008). doi:10.1016/j.msea.2008.01.013
51. C. Boehlert, D. Dickmann, N. N. Eisinger, The effect of sheet processing on the microstructure, tensile, and creep behavior of INCONEL alloy 718. *Metall. Mater. Trans., A Phys. Metall. Mater. Sci.* **37**, 27–40 (2006). doi:10.1007/s11661-006-0149-0
52. G. Liu, G. J. Zhang, F. Jiang, X. D. Ding, Y. J. Sun, J. Sun, E. Ma, Nanostructured high-strength molybdenum alloys with unprecedented tensile ductility. *Nat. Mater.* **12**, 344–350 (2013). doi:10.1038/nmat3544 Medline
53. Y. Nakamoto, M. Yuasa, Y. Chen, H. Kusuda, M. Mabuchi, Mechanical properties of a nanocrystalline Co–Cu alloy with a high-density fine nanoscale lamellar structure. *Scr. Mater.* **58**, 731–734 (2008). doi:10.1016/j.scriptamat.2007.12.013
54. T. Ungár, S. Ott, P. Sanders, A. Borbély, J. Weertman, Dislocations, grain size and planar faults in nanostructured copper determined by high resolution X-ray diffraction and a new procedure of peak profile analysis. *Acta Mater.* **46**, 3693–3699 (1998). doi:10.1016/S1359-6454(98)00001-9
55. T. Ungár, I. Dragomir, A. Revesz, A. Borbély, The contrast factors of dislocations in cubic crystals: The dislocation model of strain anisotropy in practice. *J. Appl. Cryst.* **32**, 992–1002 (1999). doi:10.1107/S0021889899009334

56. N. H. van Dijk, A. Butt, L. Zhao, J. Sietsma, S. Offerman, J. Wright, S. Vanderzwaag, Thermal stability of retained austenite in TRIP steels studied by synchrotron X-ray diffraction during cooling. *Acta Mater.* **53**, 5439–5447 (2005). doi:10.1016/j.actamat.2005.08.017
57. S. Floreen, The physical metallurgy of maraging steels. *Metall. Rev.* **13**, 115–128 (1968). doi:10.1179/mtlr.1968.13.1.115
58. Y. G. Kim, G. S. Kim, C. S. Lee, D. N. Lee, Microstructure and mechanical properties of a cobalt-free tungsten-bearing maraging steel. *Mater. Sci. Eng.* **79**, 133–140 (1986). doi:10.1016/0025-5416(86)90396-4

## ACKNOWLEDGMENTS

The authors thank Prof. K. Lu for his insightful and constructive comments on this paper. M.X. Huang is grateful for financial support from Research Grants Council of Hong Kong (Grants No. 712713, 17203014, 17255016), Natural Science Foundation of China (Grant No. U1560204). H.W. Luo is grateful for financial support from Natural Science Foundation of China (Grant No. U1460203). H.W. Yen acknowledges the Ministry of Science and Technology of Republic of China for providing financial support under Contract MOST-104-2218-E-002-022-MY3 and for the technical support from JSM 7800F PRIME at the Instrumentation Center, National Taiwan University, Taiwan. The authors also acknowledge the Shanghai Synchrotron Radiation Facility (SSRF) for providing the synchrotron XRD facility at beamline no. 14 B. M. The present work is related pending patents with an application numbers of 201610455155.3 and PCT/CN2016/096509, and another awarded patent with a number of 201410669029.9. Huang supervised the study. M. Huang, B. He and H. Luo designed the study. B. He and B. Hu prepared the thermomechanical treatment and the mechanical tests. H. Yen, G. Cheng and B. He conducted the microstructure characterization. B. He, M. Huang and H. Luo analyzed the data. Z. K. Wang discussed the results. B. He and M. Huang wrote the paper. The authors declare no competing financial interests. Data is available in the manuscript and supplementary materials.

## SUPPLEMENTARY MATERIALS

www.sciencemag.org/cgi/content/full/science.aan0177/DC1
Materials and Methods
Supplementary Text
Figs. S1 to S14
References (*54*–*58*)

20 February 2017; accepted 10 August 2017
Published online 24 August 2017
10.1126/science.aan0177

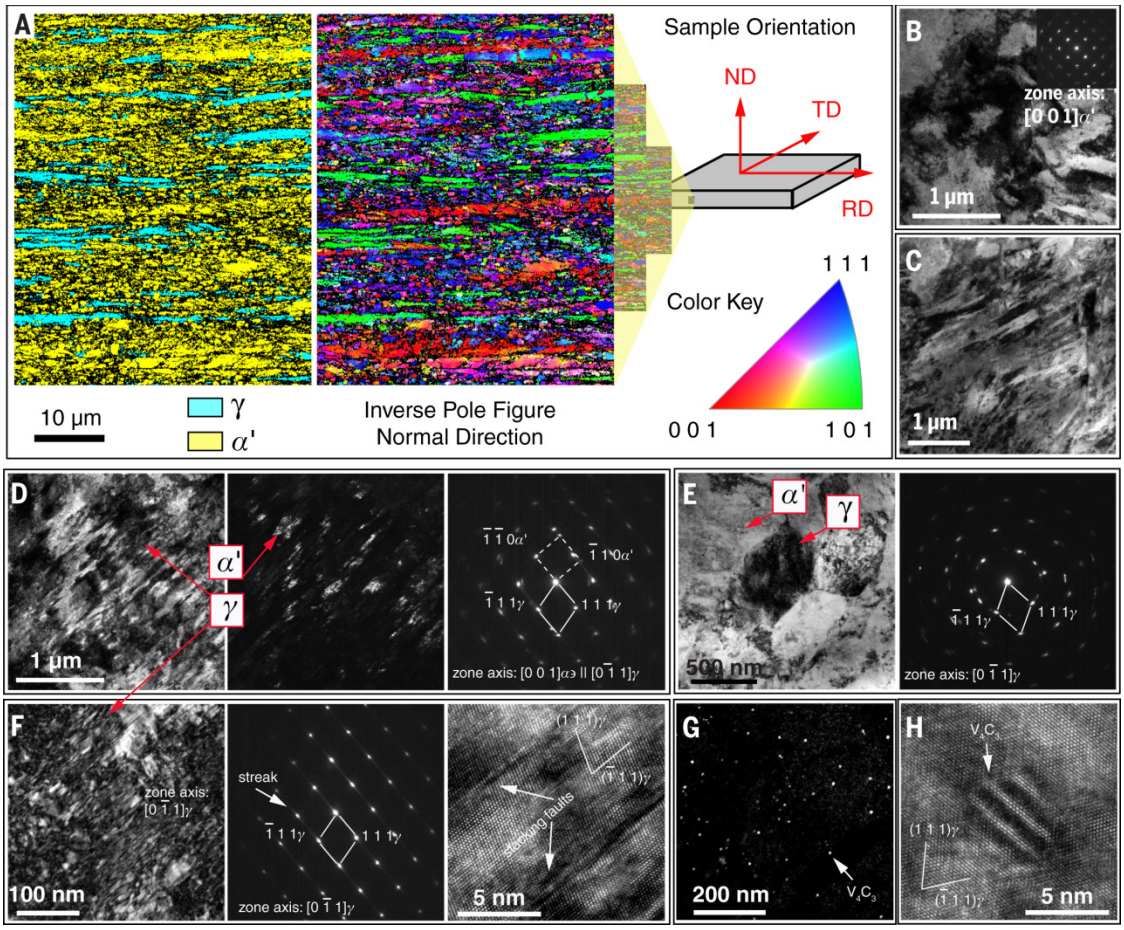


**Fig. 1. Microstructure of our D&P steel prior to the tensile test.** (**A**) Electron backscatter diffraction (EBSD) phase image and orientation image showing the lamella microstructure of austenite ($\gamma$) embedded in tempered martensite ($\alpha'$) matrix. The austenite area fraction is 15%, and the martensite area fraction is 85%. RD represents the rolling direction, ND indicates the normal direction, and TD is the transverse direction. (**B**) Dislocation structures in martensite. The upper right inset is a selected-area diffraction pattern (SADP). (**C**) A typical lenticular martensite distributed with twins and dislocations. (**D**) The lath martensite and lamella austenite as observed in transmission electron microscopy (TEM) bright-field and dark-field images. The right image is a SADP showing a Kurdjumov-Sachs (K-S) relation between lamella austenite and lath martensite. (**E**) Dislocations in sub-micron granular austenite. (**F**) Dislocations and stacking faults in a large austenite grain captured by TEM bright-field and high-resolution images. (**G**) Distribution of nano-sized vanadium carbide in tempered martensite matrix. (**H**) High-resolution TEM image of nano-sized vanadium carbide in austenite.

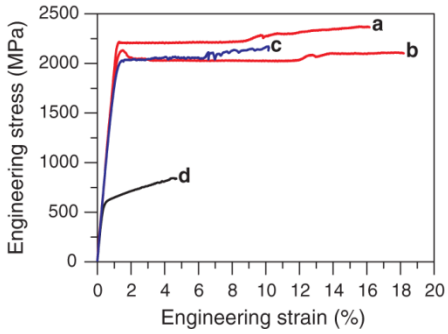


**Fig. 2. Engineering stress-strain curves of our steels at room temperature.** Curves a and b represent the D&P steels, processed by warm rolling+intercritical annealing+cold rolling (WR+IA+CR) followed by tempering at 400°C for 6 min and 15 min, respectively. Curve c represents the deformed steel, processed by WR+IA+CR without tempering at 400°C. Curve d represents the sample with bimodal coarse-grained microstructure (fig. S5) obtained by annealing at 900°C for 30 min. The uniform elongation is almost the same as the total elongation for all tensile curves. An increased yield strength of 180 MPa in curve a as compared to that in curve c is due to the segregation of C atoms at dislocations during the tempering at 400°C (*24*). The serrations at elongations between 10% and 14% in curves a and b manifest the Portevin-Le Châtelier effect (*35*).

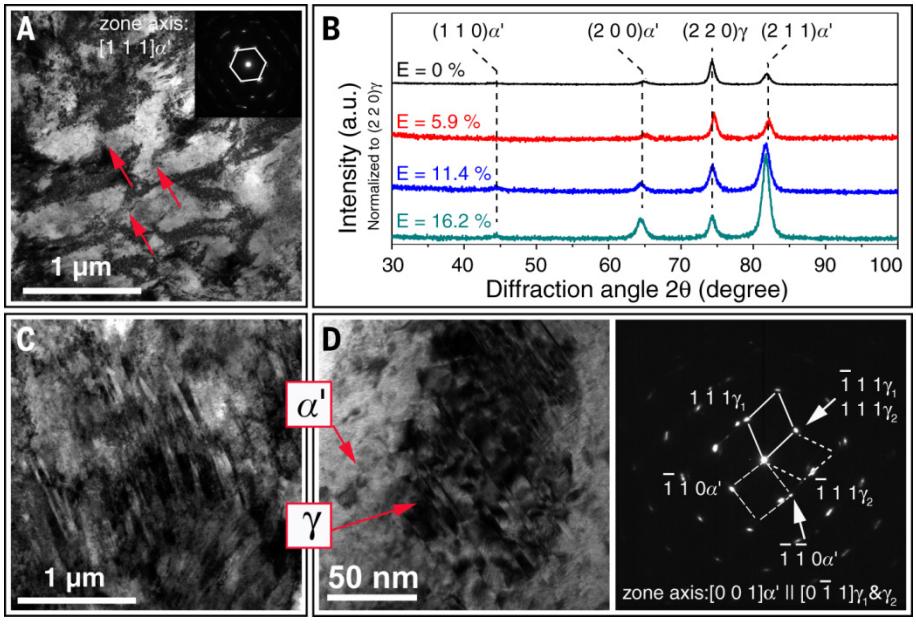


**Fig. 3. Microstructure of our D&P steel after the tensile test.** (**A**) The elongated dislocation cell structure in the tempered martensite matrix after tensile straining to 8%. The upper right inset is the corresponding selected-area diffraction pattern. Arrows mark the break of cell boundaries. (**B**) The XRD profiles at different strains. Note that the XRD measurement on the specimen of 5.9% strain is on the gauge part swept by Lüders band. Compared to the $(220)_\gamma$ peak, the significantly enhanced $(211)_{\alpha'}$ peak intensity at strains beyond 5.9% suggests that martensitic transformation is active in the large-strain regime. The abbreviation "au" represents arbitrary units. (**C**) The formation of lenticular martensite in the coarse austenite grains after tensile straining to fracture. (**D**) The generation of deformation twins in the sub-micron austenite grains after tensile straining to fracture. The right image is the SADP showing a K-S relation between twinned lamella austenite and lath martensite.

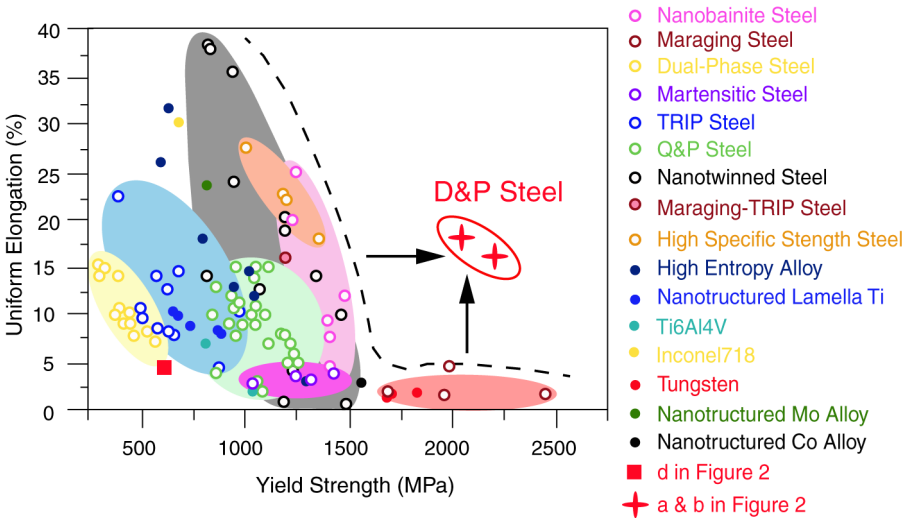


**Fig. 4. Tensile properties of our steel compared with those of other existing high strength metallic materials.** These include nanobainite steel (*36*), maraging steel (*37*, *38*), dual-phase (DP) steel (*39*), martensitic steel (*40*), TRIP steel (*41*, *42*), quenching and partitioning (Q&P) steel (*43*), nanotwinned steel (*44*, *45*), maraging-TRIP steel (*46*), high specific strength steel (HSSS) (*47*), high entropy alloys (*48*, *49*), nanostructured lamella Ti (*3*), Ti6Al4V (*47*), tungsten (*50*), Inconel 718 (*51*), nanostructured Mo alloy (*52*) and nanostructured Co alloy (*53*). Our D&P steel is clearly separated from the general trend and, therefore defines a new space in the strength-ductility map. Note the uniform elongation is selected here not only because it is a desirable property, but also because it is less affected by the sample dimensions used in different studies (*2*).

# High dislocation density–induced large ductility in deformed and partitioned steels

B. B. He, B. Hu, H. W. Yen, G. J. Cheng, Z. K. Wang, H. W. Luo and M. X. Huang

published online August 24, 2017



*Science* (print ISSN 0036-8075; online ISSN 1095-9203) is published by the American Association for the Advancement of Science, 1200 New York Avenue NW, Washington, DC 20005. 